Deformation of the Miura-Ori Patterned Sheet

Article *in* International Journal of Mechanical Sciences · May 2015

DOI: 10.1016/j.ijmecsci.2015.05.009

CITATIONS
33

READS
977

4 authors, including:

Sicong Liu
Nanyang Technological University
6 PUBLICATIONS **66** CITATIONS
SEE PROFILE

Guoxing Lu
Swinburne University of Technology
276 PUBLICATIONS **4,827** CITATIONS
SEE PROFILE

Deformation of the Miura-ori Patterned Sheet

Sicong Liu[1], Guoxing Lu[1*], Yan Chen[2] and Yew Wei Leong[3]

[1]Nanyang Technological University, 50Nanyang Ave, Singapore 639798
[2]TianJin University, 92 Weijin Rd, Nankai, Tianjin, China 300072
[3]Institute of Materials Research and Engineering, 3, Research Link, Singapore 117602

Abstract

In this paper, a Miura-ori patterned sheet was made from copolymer Elvaloy by compression molding and its deformation behavior is investigated experimentally and using finite element analysis. The intrinsic mechanical properties of Elvaloy were obtained by tensile and four-point-bending tests, respectively, and they were subsequently used in the finite element (FE) simulation. Three types of tests were conducted: out-of-plane compression, the three-point-bending and the in-plane compressions in the two directions. FE simulations using ABAQUS/Explicit were carried out to analyse the deformations of the patterned sheet under the same loading as that in the tests. The simulation results are then compared with the tests, which show good agreements. Based on the simulation results, the deformation patterns of the patterned sheet under different loading conditions were examined, as well as the energy absorption capacities.

KEYWORDS: Rigid origami, Miura-ori patterned sheet, composite material

1 introduction

Rigid origami has attracted interests from researchers in both mathematic and engineering fields. In a rigid origami pattern the surfaces surrounded by crease lines are not allowed to stretch or bend during folding [1]. The properties of rigid foldable, flat folding and developable [2] grant the rigid origami inspired structures with a wide range of potential applications, such as the energy-absorbing thin-walled structures with origami patterns [3-6], the programmable robots with precise actuation control [7, 8], and the planar fabrication of 3-D mechanisms [9].

As one of the essential rigid origami patterns, the Miura-ori consists of identical parallelogram facets surrounding the vertices of degree 4 [10]. When the facets and crease lines are replaced with rigid panels and revolute hinges, respectively, the Miura-ori can be represented by a mechanism [11, 12]. In that case, the movement of the Miura-ori can uniquely be described kinematically [13].

Miura-ori patterned sheets can be used as core of sandwich structures. Sandwich structures are widely used in aircraft and automotive industries due to their high stiffness-to-weight ratio and configurable energy absorption performance [14, 15]. However, the drawbacks of the conventional honeycomb cores, namely, the accumulation of humidity, the complicate manufacture process and the vulnerability against impact loads, limit the applications of the sandwich structures. In comparison, the Miura-ori patterned sheets have a number of advantages, such as the open ventilation channels, the continuous manufacture process, the superior energy absorption and impact properties, etc. [16].

In recent years, the studies on the Miura-ori inspired folded cores have gained popularity. Fischer et al. [17, 18] produced and tested various folded cores with different unit cell geometries and different base materials. The base materials were tested in tension and compression to obtain their material data, which was subsequently used FE simulation. Heimbs et al. [16, 19, 20] studied the mechanical behavior under compression, shear and impact loads of the folded cores made from prepreg sheets of carbon fiber/aramid fiber. In addition, a dual-core configuration with two folded cores was investigated. Lebée and Sab [21] derived upper and lower bounds for the effective transverse shear moduli of a chevron folded core and compared it to finite element computations. Schenk and Guest [22, 23] proposed a novel manufacturing process, which uses cold gas-pressure to fold sheets into Miura-ori. Two folded metamaterials were introduced based on a stacking of individual Miura-ori layers. Wei et al. [24] analysed the Poisson's ratios of the Miura-ori metamaterial and the effective bending stiffness of the unit cell, and solved the inverse design problem for the optimal geometric and mechanical response. Zhou et al. [25] presented a parametric study on the Miura-based folded core models using the finite element method. The folded core models are compared to a honeycomb core model with the same density and height.

In this paper, commercially available material, copolymer Elvaloy, has been used to prepare the Miura-ori patterned sheet by compression molding [26]. The intrinsic mechanical properties of Elvaloy were obtained through tensile and four-point-bending tests, respectively. Mechanical tests were carried out on the patterned sheet only, which included the out-of-plane compression, the three-point-bending and the in-plane compressions in the two principal directions. FE simulations using ABAQUS/Explicit were carried out to analyse the deformations of the patterned sheet. The deformations of the patterned sheet were examined from the simulation results, as well as the energy absorption capacities.

The layout of the paper is as follows. Firstly, the geometry of the Miura-ori patterned sheet will be introduced in Section 2. Next, the experiments setup and results will be

introduced in Section 3. Section 4 proposes the FE model in ABAQUS/Explicit and verifies its validity. Section 5 concludes the paper.

2 Geometries and preparation of the Miura-ori patterned sheet

2.1 The geometry of Miura-ori

The Miura-ori pattern can be constructed by the tessellation of multiple units. A unit consists of 4 identical parallelograms, see Fig. 1 a). The mountain and valley crease lines are marked as red and blue, respectively. Due to the Miura-ori's one-DOF mobility [10], when the lengths a, b and twist angle α are given as constant, the motion of the unit only depending on the dihedral angle θ, see Fig. 1 b). According to Schenk's [22] and Klett's [27] work, the rigid folding motion of the patterned sheet can be represented as follows

$$\begin{gathered} h = a\sin\theta\sin\alpha, \quad w = 2b\frac{\cos\theta\tan\alpha}{\sqrt{1+\cos^2\theta\tan^2\alpha}}, \\ l = 2a\sqrt{1-\sin^2\theta\sin^2\alpha}, \quad u = \frac{2ab\cos\alpha}{l}, \quad \sin\left(\frac{\gamma}{2}\right) = \frac{\cos\theta}{\cos\alpha\sqrt{1+\cos^2\theta\tan^2\alpha}}, \end{gathered} \tag{1}$$

The mobility of Miura-ori pattern is shown in Fig. 1 c). Due to the anisotropy of the Miura-ori pattern, the mechanical behavior of the patterned sheet depends on the directions of the loads applied. Thus, two principal directions of the patterned sheet are defined, as direction D1 and D2. Direction D3 is the out-of-plane direction.

2.2 Fabrication of the Miura-Ori patterned sheet

The commercially available Elvaloy AC 1820 was selected, which is a copolymer of ethylene and methyl acrylate in pellet form [28]. The manufacturing process is shown in Fig. 2. First, 25.9g Elvaloy pellets were melted at a temperature of 180 degrees Celsius and compressed into a flat sheet with dimensions of approximately 99mm long, 99mm wide and 2.7mm thick after cooling, see Fig. 2 a) and b). The flat sheet was then compressed to form the patterned sheet between the male and female heated stainless steel moulds at 180 degrees Celsius, see Fig. 2 c) and d). The thickness of the patterned sheet facets, *T*, turned out to be 1.8 mm on average. Due to the adhesive nature of Elvaloy when melted, mould release agent was applied

before each moulding. The Miura-ori pattern on the mould was designed based on the model shown in Fig. 1. The dimensions are

$$\alpha = 60°, \quad a = b = 10.5\,mm, \quad \theta_0 = 54°. \tag{2}$$

Substituting the above values to Eqns. (1) gives

$$h = 7.3\,\text{mm}, \quad w = 15\,\text{mm}, \quad l = 15\,\text{mm}, \quad u = 7.5\,\text{mm}, \quad \gamma_0 = 110.9^{\circ}. \tag{3}$$

Fillets with 0.5 mm radius were added to the ridgelines for milling cutter to work. After the compressed moulding, the patterned sheet is on average 1.9 mm taller than *h*, ie. $H = 9.2\,\text{mm}$, see Fig. 2 f).

Finally, to eliminate the bubbles and inconsistent thickness, the patterned sheets were trimmed into square shape with 6 units in direction D2 and 5 and half units in direction D1, see Fig. 2 e). After trimming, the average lengths of the patterned sheet in directions D1 and D2 are $L_{\text{D1}} = 88.3\,\text{mm}$, $L_{\text{D2}} = 88.4\,\text{mm}$.

3 Experiments

Two types of experiments were performed for the Elvaloy flat sheets: uniaxial tensile tests for stress-strain curves and four-point bending tests. For the patterned sheets, two types of experiments were conducted, i.e., compression tests in the global three directions of the patterned sheet and three-point bending tests.

3.1 Tests for properties of Elvaloy flat sheet

3.1.1 Tensile test

Tensile tests with Elvaloy dumbbell samples were performed according to ASTM D638, in order to characterise the mechanical property of Elvaloy. The diameter of the dumbbell is depicted in Fig. 3 a). The load-displacement data were obtained, which was then converted into the true stress-strain curve. A typical stress-strain curve is shown in Fig. 3 b). The modulus of elasticity was obtained by fitting the initial linear portion of the curve, which is 18.6 MPa, see Fig. 3 c).

3.1.2 Four-point bending test

According to the standard test method for flexural properties ASTM D6272, the four-point bending test was performed. The diameters of the specimen and test setup are shown in Fig. 4 a). This was also to be used later in validating the material property in the finite element analysis. The load and displacement were measured, as shown in Fig. 4 b). Around the end of the test, the deformation was very large and there was some slippage observed between the specimen and the roller supports.

3.2 Tests for patterned sheets

3.2.1 Out-of-plane compression test

To evaluate the characteristics of the patterned sheet in the out-of-plane direction, compression tests were performed, together with an unloading phase. Fig. 5 a) shows the setup. A mirror was fixed under the transparent bottom platen at 45 degrees to the vertical so that the camera pointing to the mirror can capture the successive in-plane deformation of the specimen. To track the in-plane displacement of the vertices, the vertices were marked and reference rulers were glued on the edge of transparent platen, see Fig. 5 b). The load-displacement curve is plotted in Fig. 5 c). The curve shows approximately five stages of the deformation. From the displacement at 0 to 1.4 mm, the deformation can be considered as linear elastic, where the load increases linearly with the displacement (Stage 1). The load increases gradually from the displacement at 1.4 to 2 mm, until a plateau has reached (Stage 2). At stage 3, the load remains constant and the patterned sheet structure collapses when the flat panels started buckling. During the displacement of 4.5 to 5.9 mm, the Miura-ori structure further collapsed with some facets touching the bottom platen. The load increases rapid with the displacement. This is followed by the unloading phase after the load reached 6 KN. The patterned sheet sprang back. After the complete unloading, the patterned sheet had a permanent displacement of 1.3 mm, and is slightly larger in area. The movement of the vertices is shown in Fig 5 d, which demonstrates that the central vertex stayed still and each unit expanded evenly.

3.2.2 In-plane compression tests

In-plane compression tests were carried out for the patterned sheet to investigate its deformation behavior. The sheet was sandwiched between two smooth and transparent rigid walls spaced at 11mm, to stop possible overall buckling, (Fig. 6a). The thickness of the

loading plate was 10mm. The loading plate pushed the patterned sheet at 10mm/min in direction D1 and D2, respectively. The deformations were recorded by camera during the tests. Deformation of the sheet exhibited a feature of overall negative Poisson's ratio [29], see Fig. 6 b) and c). The load-displacement curves are plotted in Fig. 6 d). Results for D2 showed good repeatability while for D1 direction they were less so, probably due to the friction between the patterned sheet and the transparent walls. Thus, only the curves of the in-plane D1-1 and D2-1 specimens are used. The patterned sheet starts densification at about 38mm in test D2 and 52mm in test D1, which shows the folding range in D1 is larger than that in D2. After complete unloading, there was a permanent displacement of 6.1mm and 4.6mm, in D1 and D2 directions, respectively.

3.2.3 Three-point bending test

Schenk [29] carried out three-point bending experiments on the paper model of the Miura-ori, which demonstrated the static configurations of the Miura-ori under three loading conditions. In this study of our specimens, similar to Schenk's, three-point bending tests for three arrangements of setup were conducted, with the deformations mainly along D1, D2 and Diagonal directions, respectively, (Fig. 7). A rigid stylus was used to apply a point load at the centre. Due to the friction between the specimen and loading stylus, the axis of the stylus always passed through the central vertices. As shown in Fig. 7 d), the load-displacement curves appear almost linear. At the same value of displacement, the corresponding load in test D2 is twice that in test D1 and about 3.7 times in test Diagonal. After the complete unloading, there was a permanent displacement of about 1.3 mm. The deformed patterned sheets were observed to have slowly sprung back to the original shape, after the tests.

4 Finite element analysis

Commercial software ABAQUS/Explicit was employed to study the deformation of specimens under the same conditions as for the tests. Details of deformation from the finite element analysis are reported.

4.1 Validation of material constitutive model

A user defined isotropic elastic-plastic material is implemented in ABAQUS/Explicit for Elvaloy. The value of density was taken from the data sheet [28] and stress-strain curve from

the tension test (Fig. 3 c) was used. The values are density $\rho = 942\,\mathrm{kg/m^3}$ and Young's modulus $E = 18.6\,\mathrm{MPa}$. The value of Poisson's ratio was assumed $\nu = 0.35$, based on this property of other similar polymers. This material model in ABAQUS/Explicit was validated by simulating the four-point bending test, see Fig. 8 a). The specimen was modelled with 4 node quadrilateral shell element S4R, whose size was 0.5 mm. The displacement was applied to the load span and the reaction force was calculated. Fig. 8 b) shows the force-displacement curves from the simulation and test. The simulation shows good agreement with the test up to a large value of displacement.

4.2 FE simulations of patterned sheet

The patterned sheet model was first built in SolidWorks by tiling identical Miura-ori units shown in Fig. 1. Such a patterned sheet was then meshed and modelled with shell elements of type S4R in ABAQUS/Explicit. The previously defined material constitutive relation was used. In order to further validate the FE model, compression test in the out-of-plane direction was simulated. The loading and supporting platens were both treated as rigid elements (see Fig. 5 a). The bottom platen was fully fixed while the top one was used to slowly apply displacements of up to 5.9 mm, which is the same as that in the test (Fig. 5 c). Self-contact was defined, which took into account hard contact and friction between the platens and the patterned sheet. Both the reaction and the displacement of the loading plate were noted. Several modelling parameters may affect the accuracy of the simulation and their sensitivity was studied.

(1) Element size

Different mesh sizes were used as shown in Fig. 9 a), and Fig. 9 b) plots the load-displacement curves obtained from FE. A smaller element size of 1.0 mm resulted in a reduced force compared that for 1.2mm size, but the CPU time increased significantly. Further refinement to 0.8mm did not seem to improve the accuracy significantly. Hence an element size of 1 mm was selected as the default element size for all the subsequent simulations.

(2) Loading rate

In order to simulate the quasi-static experiments in the FE analysis with an acceptable computing time, the loading rate in the simulation has to be considerably higher than that

employed in the tests to reduce the CPU time, while the kinetic energy generated during the simulation should be lower than 5%. Therefore, a compression speed of 20, 25, 50 mm/s was applied, respectively, and their corresponding results are compared in Fig. 9 c). The force seems not sensitive to the loading rates for most values of displacement, though a speed of 20mm/s gave the lowest value of the force. Subsequently, 20mm/s was chosen as the compression speed of the top platen.

(3) Friction

In the out-of-plane compression test, the patterned sheet tends to expand in D1 and D2 directions when compressed by the loading platen in the D3 direction. The friction between sheet and the two platens resists this relative movement. Fig. 9 d) shows the FE load-displacement curves for three different value of coefficient of friction. As expected, the force increases with the value of friction coefficient. A friction coefficient of 0.3 gives reasonable agreements with the test (Fig. 10) and hence was used.

4.3 FEA results

After validation of the FE model, FE simulations were performed for the in-plane compression and three-point bending tests. The FE models were set up as shown in Figs. 6 and 7. Except for the patterned sheet, all the parts in the simulations were defined as rigid. The supporting parts were completely fixed. Self-contact was defined, including hard contact and friction. The reaction forces and displacements at the reference points of the loading parts were obtained. In the in-plane compression simulations, the patterned sheet model was compressed in D1 and D2 directions at displacements 55 mm and 50 mm, respectively, matching the test data shown in Fig. 6 d). In the three-point bending simulations, the loading stylus, whose axis went pass the central vertex, was displaced 15 mm in D3 direction corresponding to the test data in Fig. 7 d).

The simulation results are shown in Figs. 11 and 12. The simulation result of the in-plane D1 compression fits closely to the test data in the overall energy absorption and elastic section, see Fig. 11 c). It shows a softer behavior in the plastic section and unloading which is ascribed to less accumulated structure compared to the test sample. The simulation for the in-plane compression D2 shows only comparable trend in the force-displacement curve but smaller reaction force value compared with the test data, which can be ascribed to the lack of

thickness in the shell elements. The adjacent facets of the patterned sheet in the tests initiated interactions at a small displacement, while virtually untouched in the FE model.

In the three-point bending simulations, the simulation result shows acceptable consistency with the test data, see Fig. 12.

5 Discussion

5.1 Deformations

Corresponding to the test curve, the curve obtained from the FE simulation of the out-of-plane compression shows similar five stages as shown in Fig. 10 b), which can be related to the deformation phenomena of the patterned sheet, see Fig. 13 a).

In the linear elastic stage from the displacement at 0 to 1 mm, the dihedral angle γ increases while θ decreases, as a result, the patterned sheet expands slightly. In stage 2, from the displacement at 1 to 1.8 mm, the facets started to deform. In stage 3, from the displacement at 1.8 to 4.1 mm, the buckling of the facets turns the mountain and valley ridgelines of each unit into rotational symmetrical J shapes. During the displacement of 4.1 to 5.9 mm, after the facets touching with the platens, the structure of the patterned sheet collapses and the densification begins. In the unloading stage, the compactly compressed patterned sheet springs back together with the loading platen to the height which is 2.2 mm lower than the original. However, the changes of the shape after the test are less than that in the simulation.

Compared with the deformation in the out-of-plane compression, the deformations in in-plane compression simulations display less bending on the facets. In the beginning of in-plane compression D1, see Fig. 13 b), the dihedral angle γ decreases at first while angle θ increases, which corresponding to the waist shape of the patterned sheet in the middle of the compression (Fig. 11 a). Then angle γ returns to its original value whilst angle θ reaches its maximum value and the structure is compactly compressed. In the simulation of the in-plane compression D2 (Fig 13 c), the dihedral angle γ always decreases with θ's increase until compactly compressed.

By checking the PEEQ plot of the three-point bending simulations in ABAQUS, there are no plastic deformations took place on the patterned sheet. The deformation patterns of the center unit are shown in Fig. 14. Compared with its original shape, the unit deforms to the

largest when the displacement is at 15mm. In the simulation for D2, the distance V2V5 decreases, while V1V4, V3V6, V1V3 and V4V6 increases, see Fig. 14 a) and c). In the simulation for D1, V1V3 and V4V6 extend almost the same as in simulation D2, but distances V1V4, V2V5 and V3V6 change less, see Fig, 14 b). In the simulation for Diagonal, the unit deforms the least, see Fig. 14 d).

The typical MISEs plots of the patterned sheets in all the simulations are shown to check the distributions of stress. It's apparent that in Fig. 15 a), the valley ridgelines in touch with the supporting platen contribute the most to the reaction force in the out-of-plane compression. In the in-plane compression D1, the mountain ridgelines parallel to D1 contribute the most to the reaction force, see Fig. 15 b). The reaction force in the in-plane compression D2 mainly generated from the folding of all the ridgelines, see Fig. 15 c). In the three-point bending simulations, it appears that the stress concentrates on the center unit in D2 simulation, see Fig. 15 e). In simulations D1 and Diagonal, three rows of units in the middle deform the most, see Fig. 15 d) and f), respectively.

5.2 Energy absorption

Due to the natural of Elvaloy, the patterned sheet can be compactly compressed and springs back without destroying its structure. The absorbed energy results in the dimension changes and hardening of the patterned sheet after recovery. Before densification, the patterned sheet absorbs the most energy under out-of-plane compression with a displacement about half of its height, the force-displacement curve in Fig. 8 shows a smooth and constant behavior, especially when the buckling is undergoing. On the other hand, in the in-plane compression tests, the patterned sheet can be compressed about 60% and 40% of its length respectively in D1 and D2 direction before densification. The patterned sheet absorbs 50% more energy in the in-plane D1 direction than D2. According to the PEEQ plot of the patterned sheet in the simulations for three-point bending tests, the patterned sheet exhibits no plastic deformations, which limited the prediction of its energy absorption capacity in such loading situation.

5.3 Parallel parameter study

For potential applications, the mechanical behavior of the patterned sheet can be design to meet a range of specific requirements. To provide design instruction, parallel parameter studies on the thickness of the facet T and angle α of the patterned sheet were carried out

independently utilizing the established FE model. The other parameters of the unit in the patterned sheet are still set as the previous, as well as the same tessellation of the units. The dimensions of the patterned sheet with different values of α are listed in Table 1.

Table 1 Dimensions of the patterned sheets

α (degree)	30°	50°	70°	80°
L_{D1} (mm)	115.2	98.9	80.6	72.8
L_{D2} (mm)	40.5	72.3	107.1	120.7
h (mm)	4.2	6.5	8.0	8.4

In the out-of-plane and in-plane compression simulations on patterned sheets with different *T*, it's obvious that the patterned sheet of larger thickness, among 1.5 mm, 2 mm and 2.5 mm, generates greater reaction force to resist compressions (see Fig. 16 a, b and c). For the patterned sheets with different α, the simulation results show that smaller α leads to a stronger structure in all three directions of compressions (see Fig. 16 d e and f). The patterned sheets of larger α generate lower reaction forces in the out-of-plane and in-plane D1 compressions, whilst increase the stiffness in the in-plane D2 compressions.

When angle α is too smaller or large, $\alpha = 30^\circ$ or $\alpha = 80^\circ$ as shown in Fig. 16 e) and f), the patterned sheets become unstable in the in-plane direction D1 or D2, respectively. Under in-plane D1 compression as shown in Fig. 16 g), the sheet of angle $\alpha = 30^\circ$ intends to buckle in the out-of-plane direction, which was stopped by the walls. It subsequently started local densification at the side close to the loading plate. When subjected to in-plane D2 compress as shown in Fig. 16 h), the sheet of angle $\alpha = 80^\circ$ twists around two centers, which buckle first, instead of contracting in D2 direction. Thus, in these extreme cases, new tessellation configurations are needed to make the sheet stable under in-plane compressions.

6 Conclusion

The Miura-ori patterned sheet has been made from commercialized material copolymer Elvaloy by compression moulding and its deformation behavior have been investigated experimentally and using finite element analysis. The intrinsic mechanical properties of Elvaloy have been obtained through tensile and four-point-bending tests, which are used in the finite element (FE) simulation. The newly introduced in-plane compression tests along with three-point bending tests have been performed. After each tests, the patterned sheet

specimen sprang back with trivial changes of its original dimensions. Thus, the repeated usage of the patterned sheet is possible. Its light weight, commercialized material, simple manufacture process and repeat-use capability grant the Elvaloy patterned sheet with application potential as wearable equipment, such as the cushion units in sports shoes and the safety gears for construction workers. The validation of the FE model has been completed in ABAQUS/Explicit. The simulations have been carried out on the Miura-ori patterned sheet under a series of loading situations corresponding to the tests. The simulation results have been compared with the mechanical tests, which show good consistency. Based on the simulation results, the deformations of the patterned sheet under different load situation have been discussed. The energy absorption capacities of the patterned sheet have been investigated. To provide design instructions of the patterned sheet for a certain application, the parallel parameter studies on the thickness and the value of angle α have been carried out utilizing the established FE model.

REFERENCE

[1] N. Watanabe, K. Kawaguchi, The Method for Judging Rigid Foldability, Origami 4, A K Peters/CRC Press, 2009, pp. 165-174.

[2] J.M. Gattas, W. Wu, Z. You, Miura-Base Rigid Origami: Parameterizations of First-Level Derivative and Piecewise Geometries, Journal of Mechanical Design, Vol. 135, 2013, 111011.

[3] J. Song, Y. Chen, G. Lu, Axial crushing of thin-walled structures with origami patterns, Thin-Walled Structures, Vol. 54, 2012, pp. 65-71.

[4] J. Song, Y. Chen, G. Lu, Light-weight thin-walled structures with patterned windows under axial crushing, International Journal of Mechanical Sciences, Vol. 66, 2013, pp. 239-248.

[5] J. Ma, Z. You, Energy Absorption of Thin-Walled Square Tubes With a Prefolded Origami Pattern—Part I: Geometry and Numerical Simulation, Journal of Applied Mechanics, Vol. 81, 2013, 011003.

[6] J. Ma, Z. You, Energy absorption of thin-walled beams with a pre-folded origami pattern, Thin-Walled Structures, Vol. 73, 2013, pp. 198-206.

[7] A. Byoungkwon, D. Rus, Programming and controlling self-folding robots, Robotics and Automation (ICRA), 2012 IEEE International Conference, 2012, pp. 3299-3306.

[8] C.D. Onal, R.J. Wood, D. Rus, An Origami-Inspired Approach to Worm Robots, Mechatronics, IEEE/ASME Transactions, Vol. 18, 2013, pp. 430-438.

[9] C.D. Onal, R.J. Wood, D. Rus, Towards printable robotics: Origami-inspired planar fabrication of three-dimensional mechanisms, Robotics and Automation (ICRA), 2011 IEEE International Conference, 2011, pp. 4608-4613.

[10] K. Miura, Map Fold a La Miura Style, Its Physical Characteristics and Application to the Space Science, Research of Pattern Formation, KTK Scientific Publishers, Tokyo, 1989, pp. 77-90.

[11] M. Trautz, A. Künstler, Deployable folded plate structures - folding patterns based on 4-fold-mechanism using stiff plates, Symposium of the International Association for Shell and Spatial Structures, Valencia, 2009.

[12] S.C. Liu, Y. Chen, G. LU, the Rigid Origami Patterns for Flat Surface, Proceedings of the ASME 2013 International Design Engineering Technical Conferences & Computers and Information in Engineering Conference, 2013.
[13] M. Schenk, S.D. Guest, Origami folding: A structural engineering approach, Origami 5: Fifth International Meeting of Origami Science, Mathematics, and Education (5OSME), 2011, pp. 291-303.
[14] J. Shen, G. Lu, L. Zhao, Q. Zhang, Short sandwich tubes subjected to internal explosive loading, Engineering Structures, Vol. 55, 2013, pp. 56-65.
[15] G. Lu, T. Yu, Energy Absorption of Structures and Materials, Woodhead Publishing, Cambridge, UK, 2003.
[16] S. Heimbs, P. Middendorf, S. Kilchert, A.F. Johnson, M. Maier, Experimental and Numerical Analysis of Composite Folded Sandwich Core Structures Under Compression, Applied Composite Materials, Vol. 14, 2007, pp. 363-377.
[17] S. Fischer, S. Kilchert, M. Klaus, C. Cluzel, Sandwich structures with folded core: manufacturing and mechanical behavior, SAMPE Europe international conference, Paris, 2009, pp. 256-263.
[18] S. Fischer, K. Drechsler, S. Kilchert, A. Johnson, Mechanical tests for foldcore base material properties, Composites Part A: Applied Science and Manufacturing, Vol. 40, 2009, pp. 1941-1952.
[19] S. Heimbs, J. Cichosz, M. Klaus, S. Kilchert, A.F. Johnson, Sandwich structures with textile-reinforced composite foldcores under impact loads, Composite Structures, Vol. 92, 2010, pp. 1485-1497.
[20] S. Heimbs, S. Kilchert, M. Klaus, Sandwich panels with cellular cores made of folded composite material: mechanical behaviour and impact performance, 17th international conference on composite materials (ICCM-17), Edinburgh, 2009.
[21] A. Lebée, K. Sab, Transverse shear stiffness of a chevron folded core used in sandwich construction, International Journal of Solids and Structures, Vol. 47, 2010, pp. 2620-2629.
[22] M. Schenk, S.D. Guest, Cold gas-pressure folding of Miura-ori sheets, Steel Research International, Special Issue Proceedings of the International Conference on Technology of Plasticity (ICTP), 2011, pp. 459-464.
[23] M. Schenk, S.D. Guest, Geometry of Miura-folded metamaterials, Proceedings of the National Academy of Sciences, Vol. 110, 2013, pp. 3276-3281.
[24] Z.Y. Wei, Z.V. Guo, L. Dudte, H.Y. Liang, L. Mahadevan, Geometric Mechanics of Periodic Pleated Origami, Phys Rev Lett, Vol. 110, 2013, 215501.
[25] X. Zhou, H. Wang, Z. You, Mechanical properties of Miura-based folded cores under quasi-static loads, Thin-Walled Structures, Vol. 82 , 2014, pp. 296-310.
[26] H. Hamada. Y. W. Leong, Introduction to Film Insert Injection Molding: A Practical & Theoretical Approach, Lambert Academic Publishing, 2010.
[27] Y. Klett, K. Drechsler, Designing technical tessellations, In Proceedings of The 5th International Conference on Origami in Science, Mathematics, and Education (5OSME), Singapore, 2010.
[28] Elvaloy AC resins Product Data Sheet, http://www2.dupont.com/Elvaloy/en_US/assets/downloads/elvaloy_ac_1820.pdf.
[29] M. Schenk, Folded Shell Sructures, PhD Thesis, University of Cambridge, 2011.

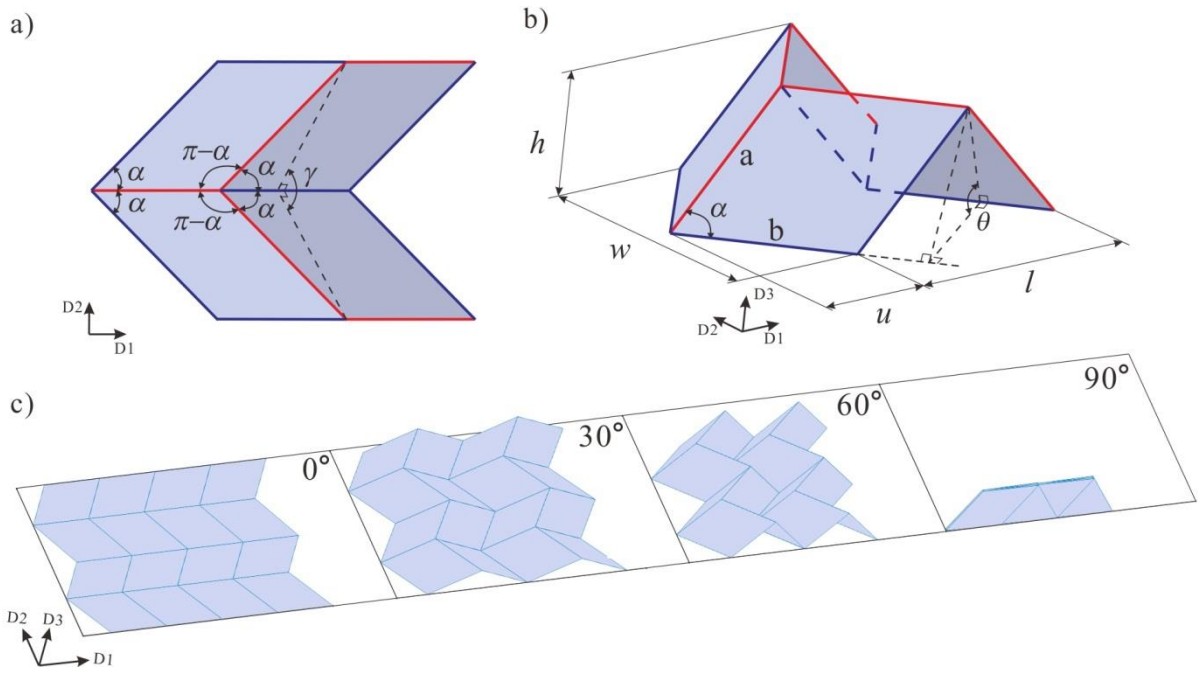

Figure 1 a) A unit of the Miura-ori pattern, b) the definition of parameters, c) the same Miura-ori pattern with different values of dihedral angle θ.

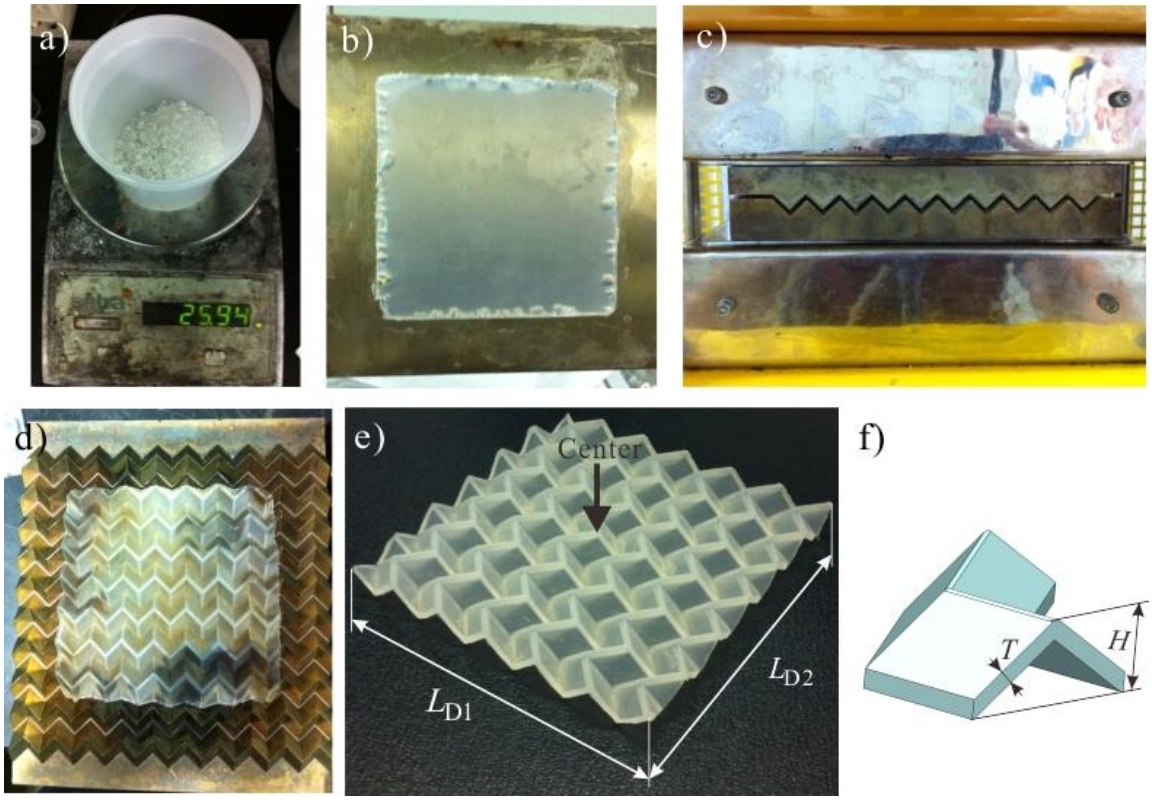

Figure 2 The manufacturing process of Miura-ori patterned sheet is as follows: a) 25.9g Elvaloy pellets were melted and b) compressed into a flat sheet, then, c) the flat sheet was compressed into Miura-ori patterned sheet in d) the heated stainless mould. e) The peripheries were trimmed, and the center and lengths of in direction D1 and D2 are measured. f) The thickness of the panels and fillet on the ridgeling are measured.

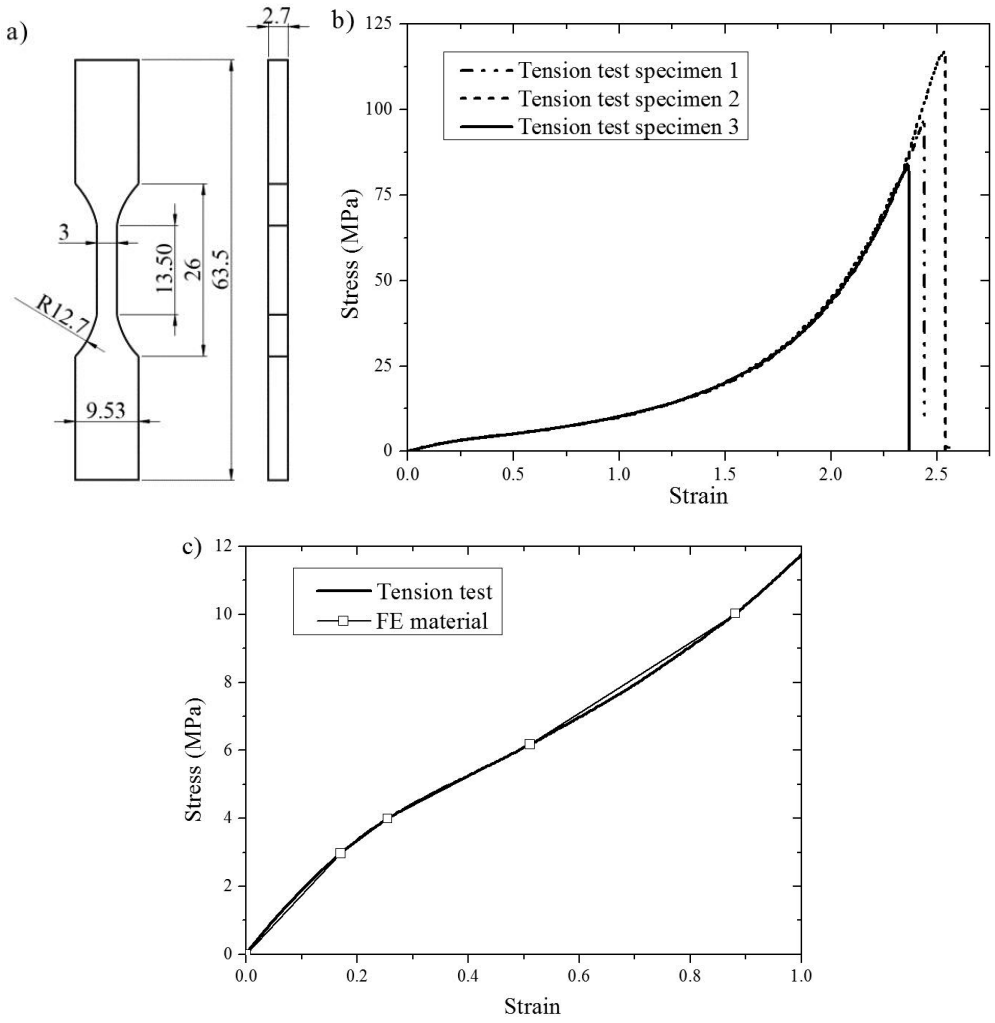

Figure 3 Tensile test: a) the dumbbell specimen; data obtained and converted to b) true stress strain, c) test result with fitted curve.

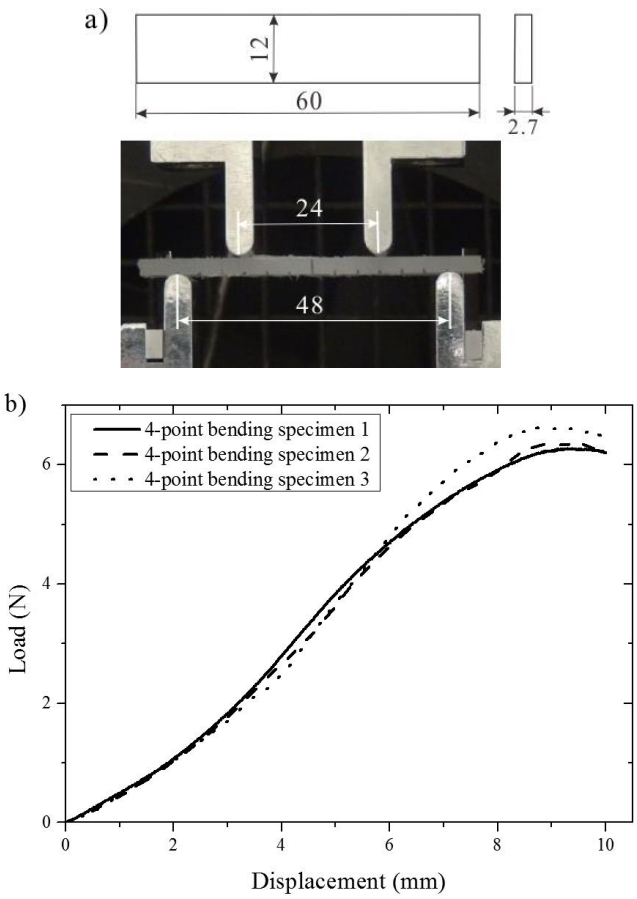

Figure 4 Four-point bending test: a) The diameter of the specimen and test setup, b) the load-displacement curve.

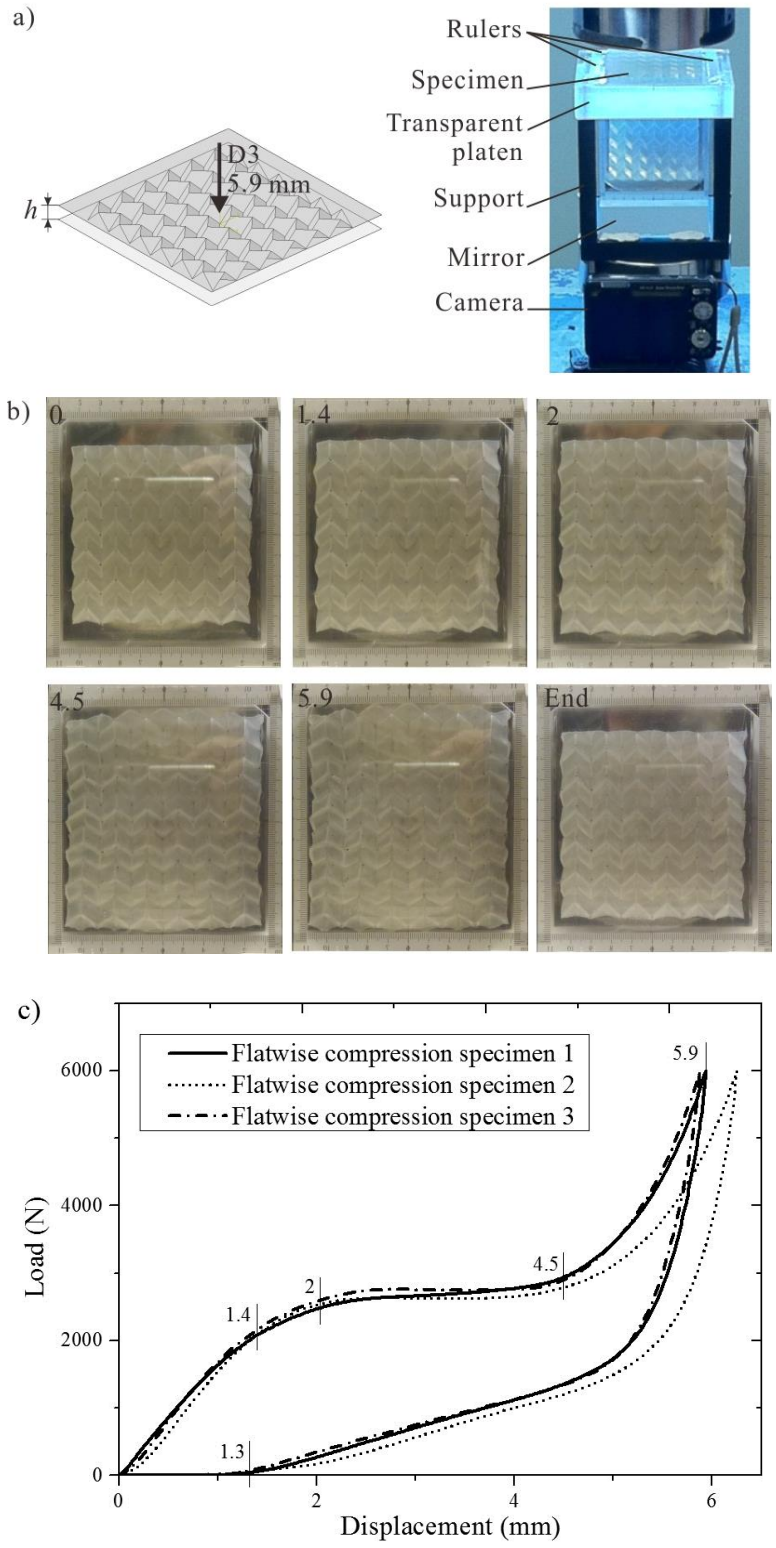

Figure 5 Out-of-plane compression: a) the setup, b) deformation of the patterned sheet, c) the load-displacement curve.

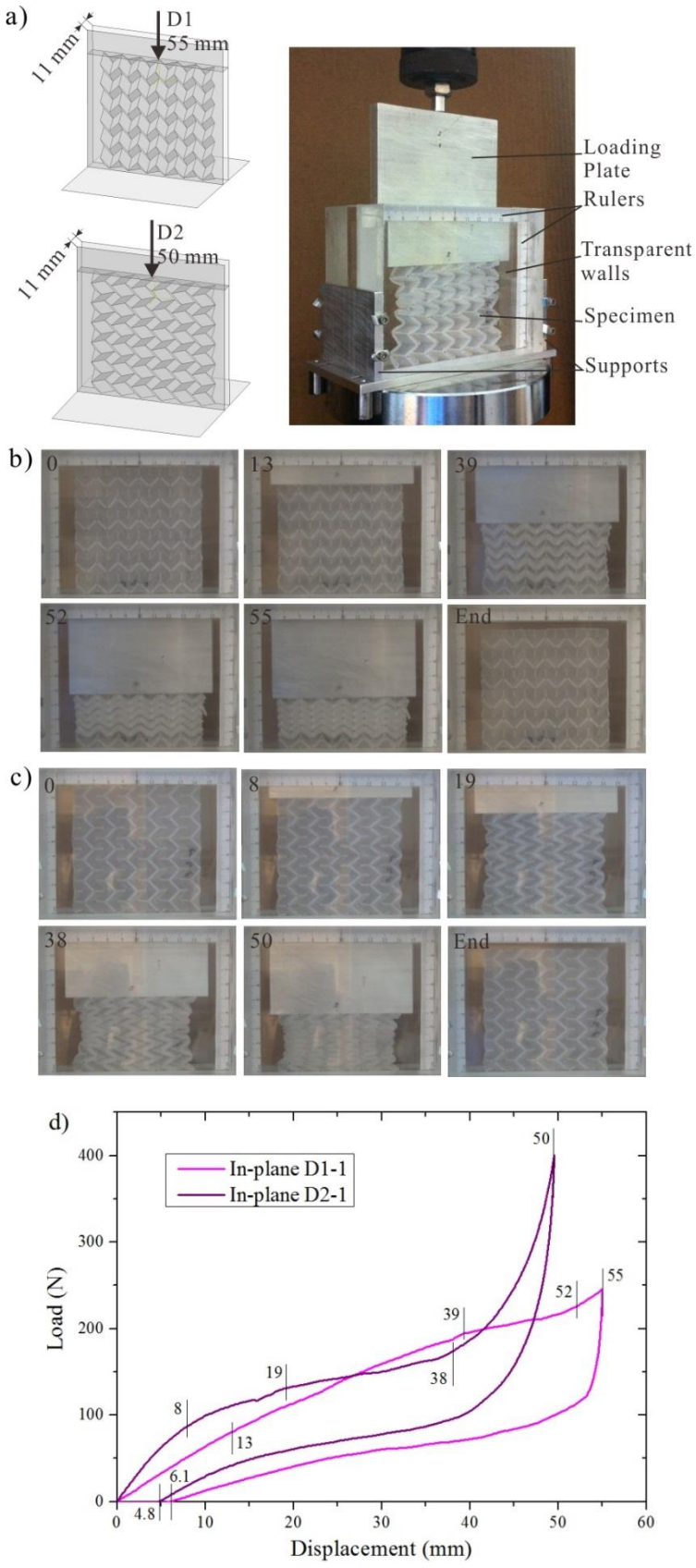

Figure 6 The in-plane compressions: a) the setup, b) test in direction D1 and c) D2, d) the load-displacement curves.

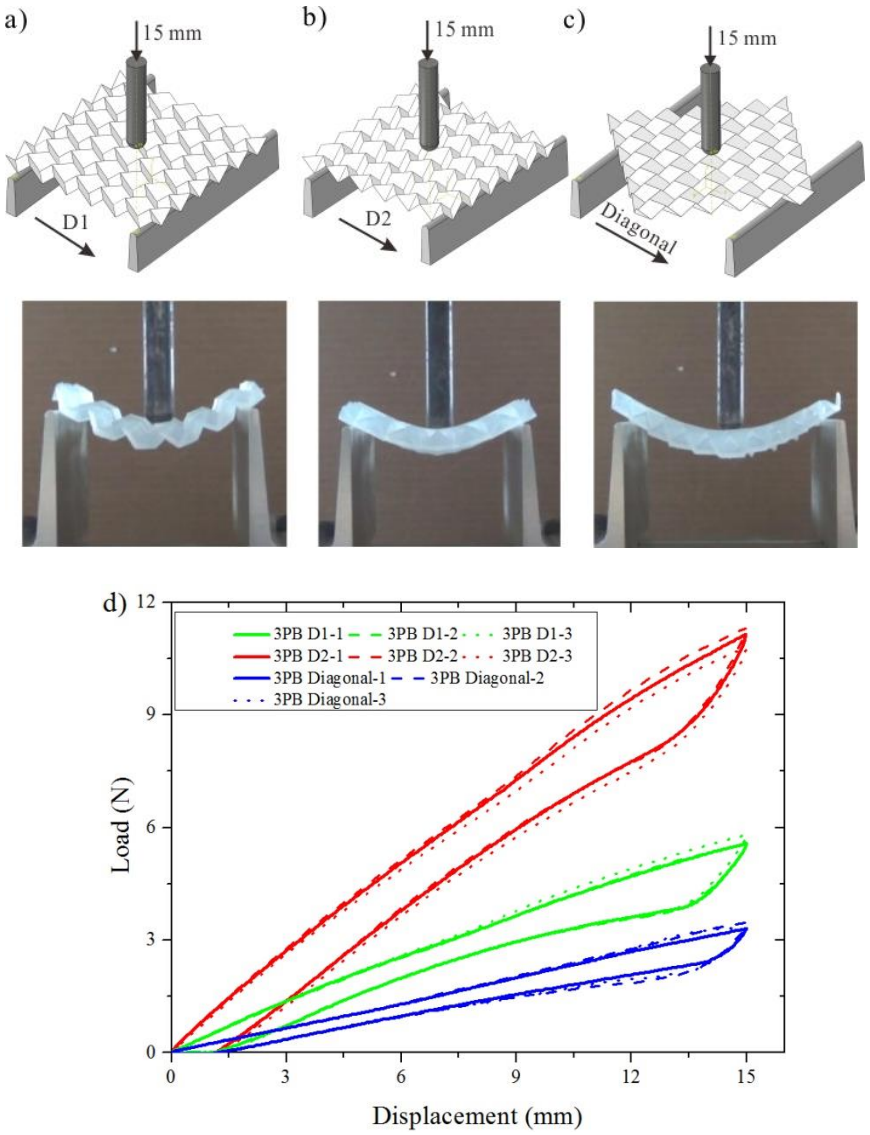

Figure 7 The Three-point bending test in directions a) D1, b) D2 and c) Diagonal; d) the load-displacement curves.

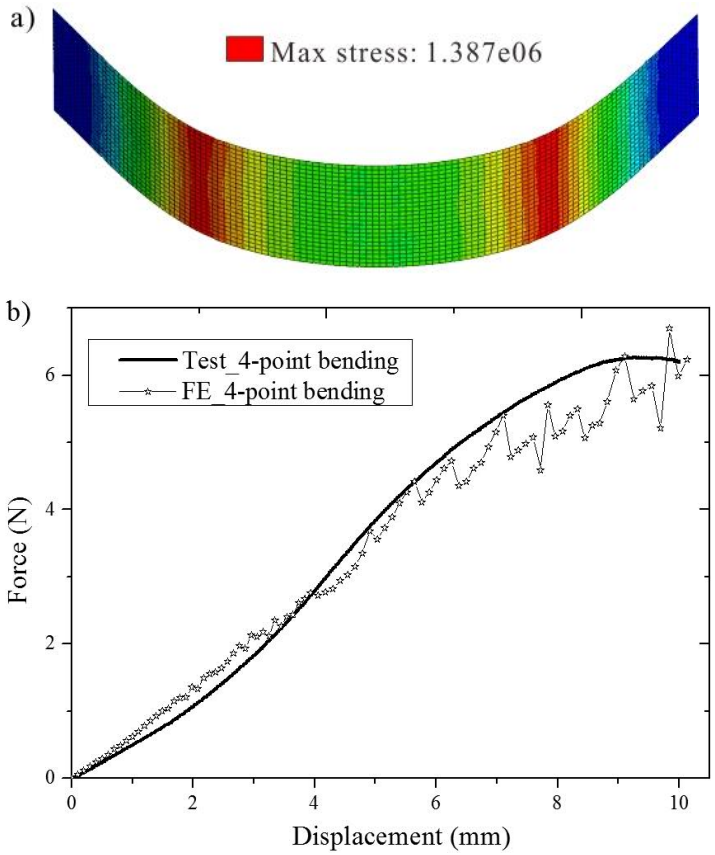

Figure 8 Validation of material model performed on the four-point bending test: a) FE model after simulation, b) the comparation between test and FE result.

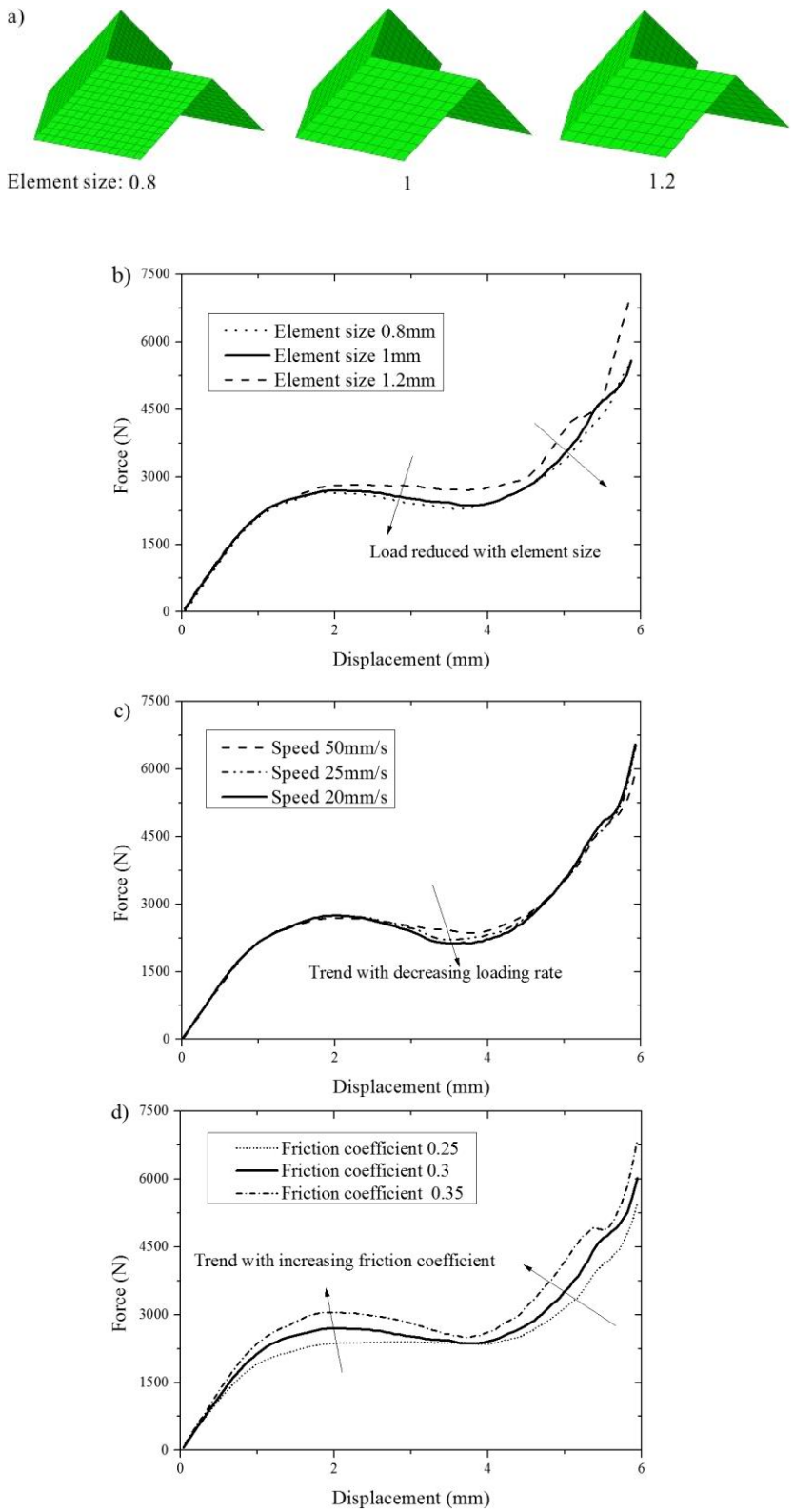

Figure 9 The influence of model parameters in the simulation of out-of-plane compression: a) different sizes of the elements are investigated; the curves of different b) element size, c) loading rates and d) friction coefficient.

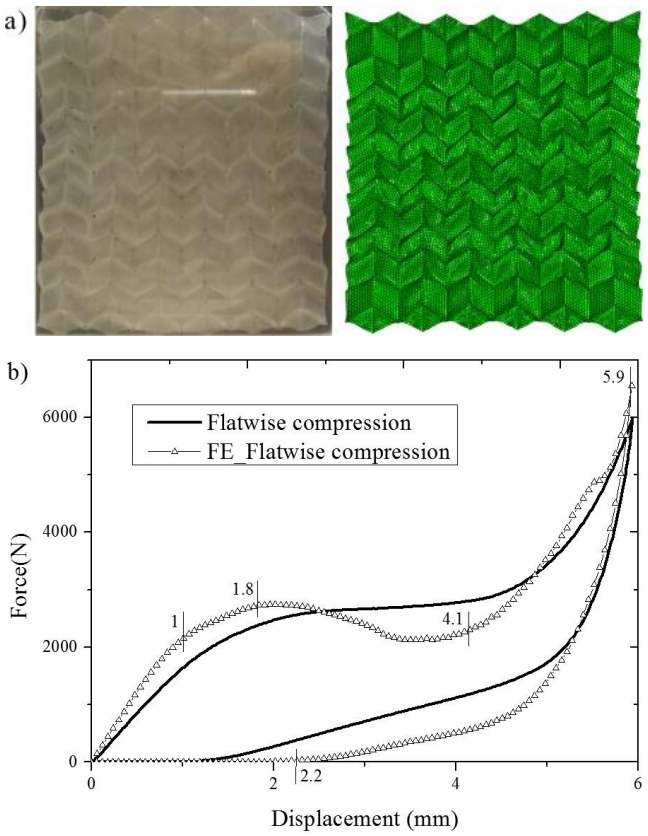

Figure 10 The simulation results of out-of-plane compression compared with test: a) deformations b) the force-displacement curves.

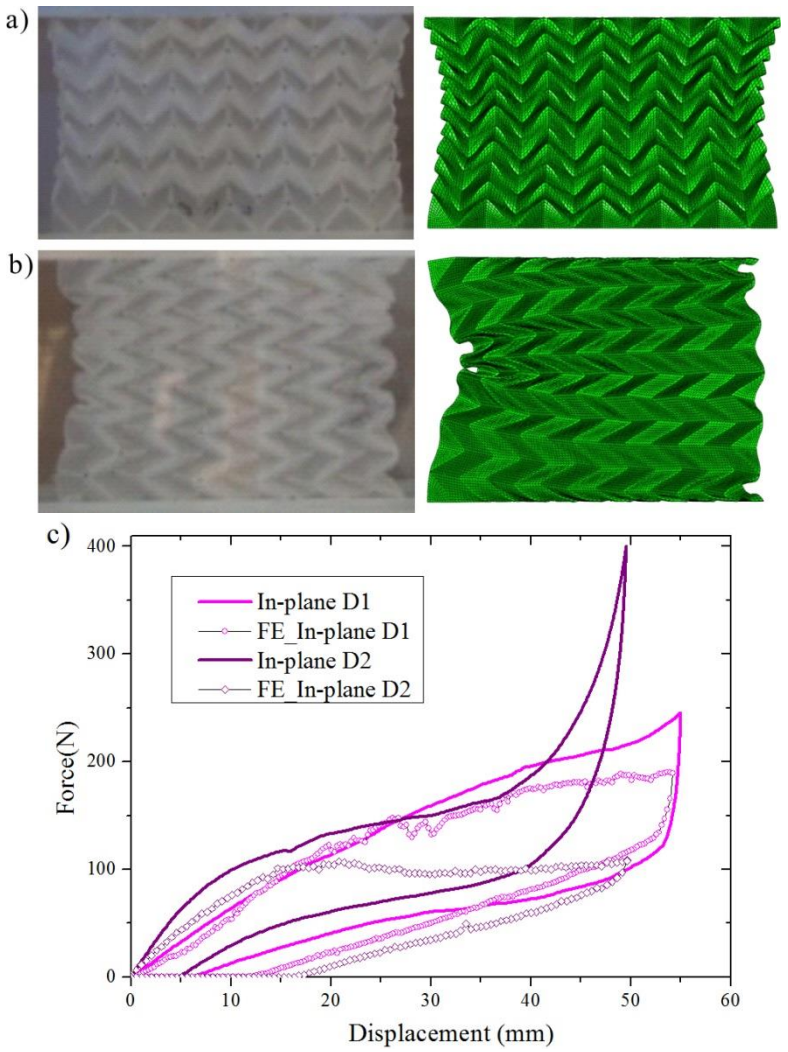

Figure11 The simulation results of the in-plane compression in a) D1 and b) D2; c) the force-displacement curves are compared with the tests.

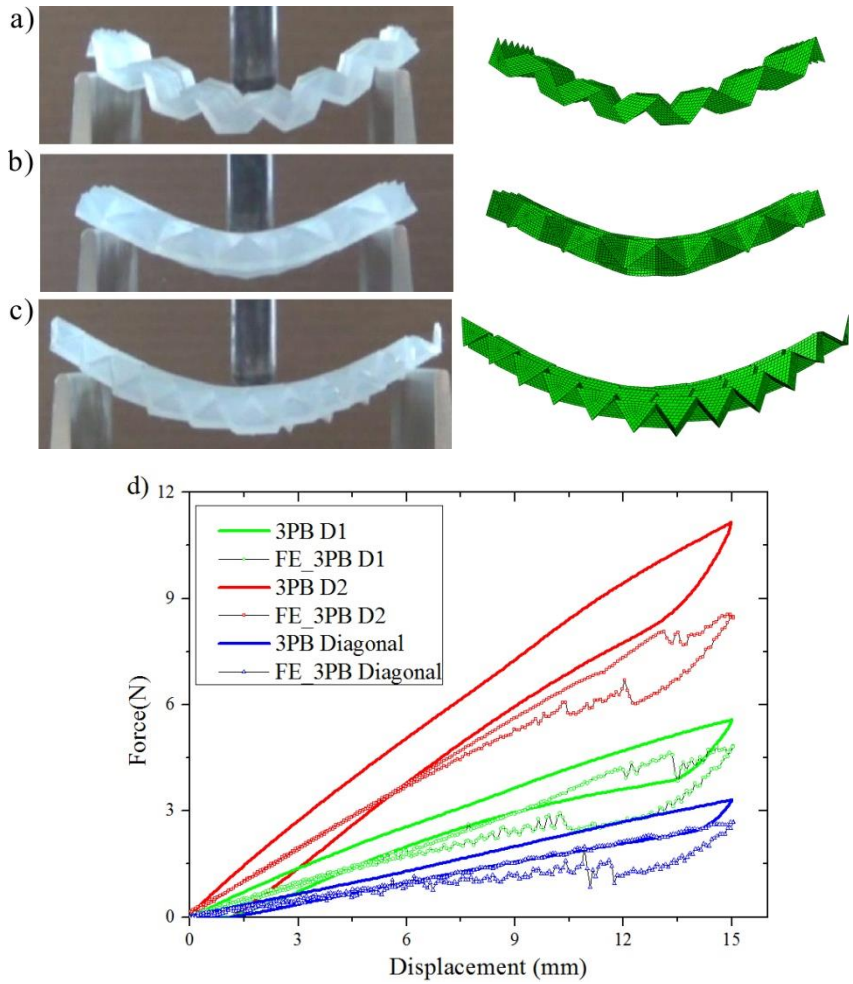

Figure12 The simulation results of three-point bending test in a) D1, b) D2 and c) Diagonal; d) the force-displacement curves are compared with the experimental results.

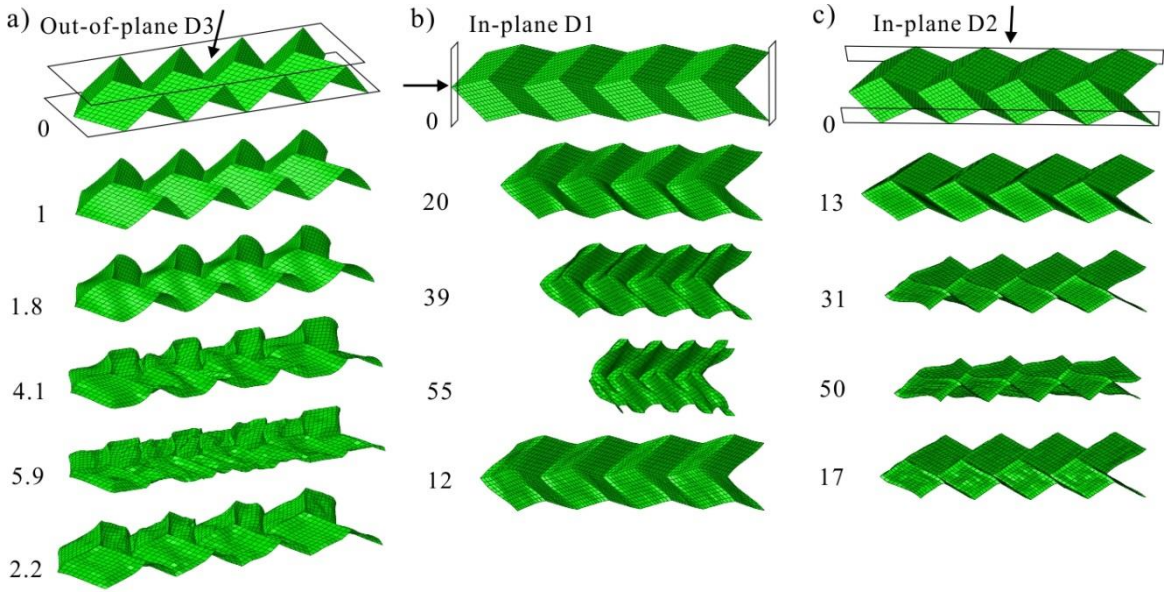

Figure 13 The typical deformation in simulations: a) out-of-plane compression, in-plane compression b) D1, c) D2.

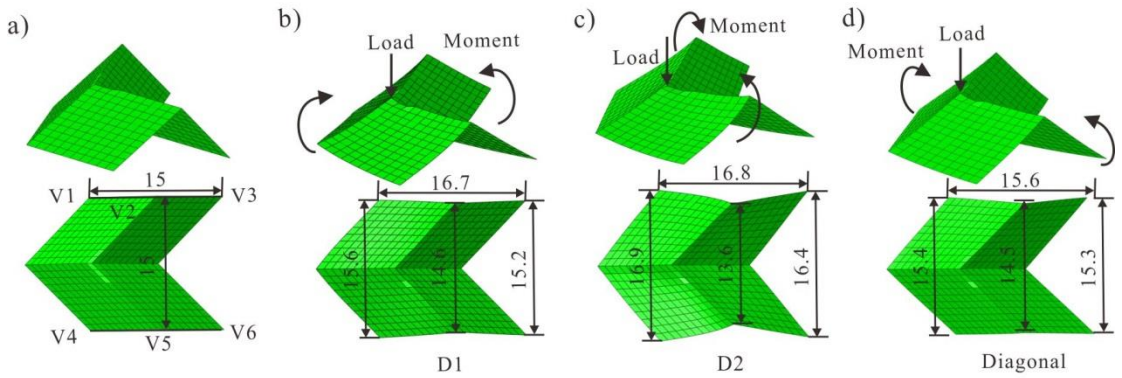

Figure 14 a) The original shape of the center unit, the largest deformations of the center units in simulations of three-point bending b) D1, c) D2 and d) Diagonal.

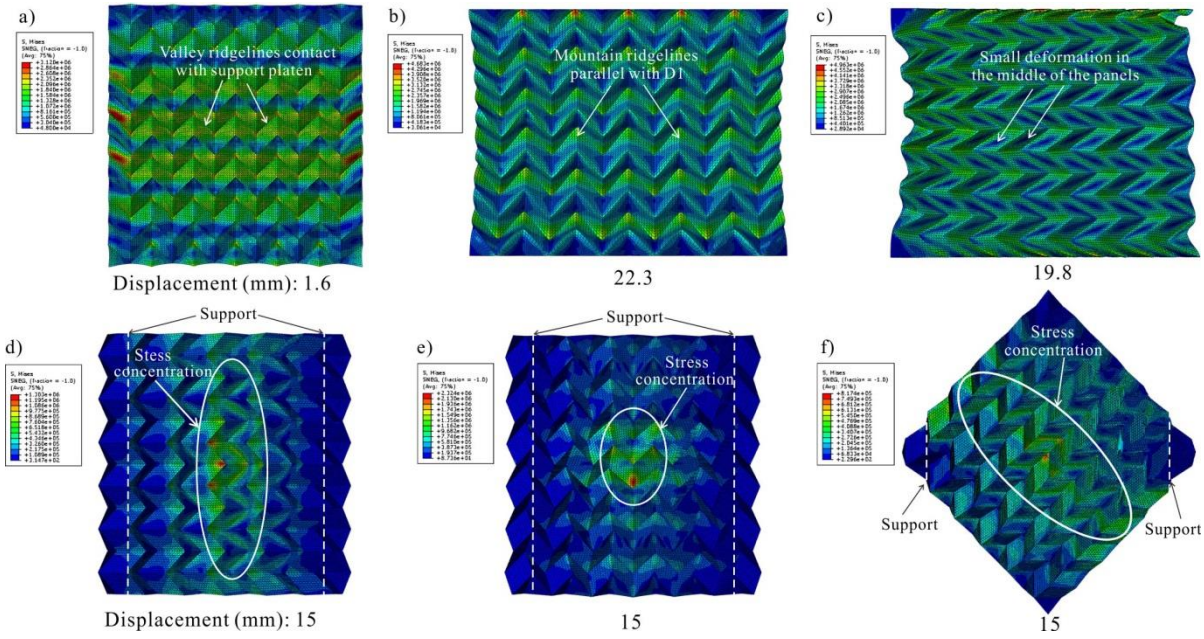

Figure 15 The MISEs plot of the patterned sheet in simulations: a) out-of-plane compression; b) in-plane compression D1 and c) D2; three-point bending d) D1, e) D2 and f) Diagonal.

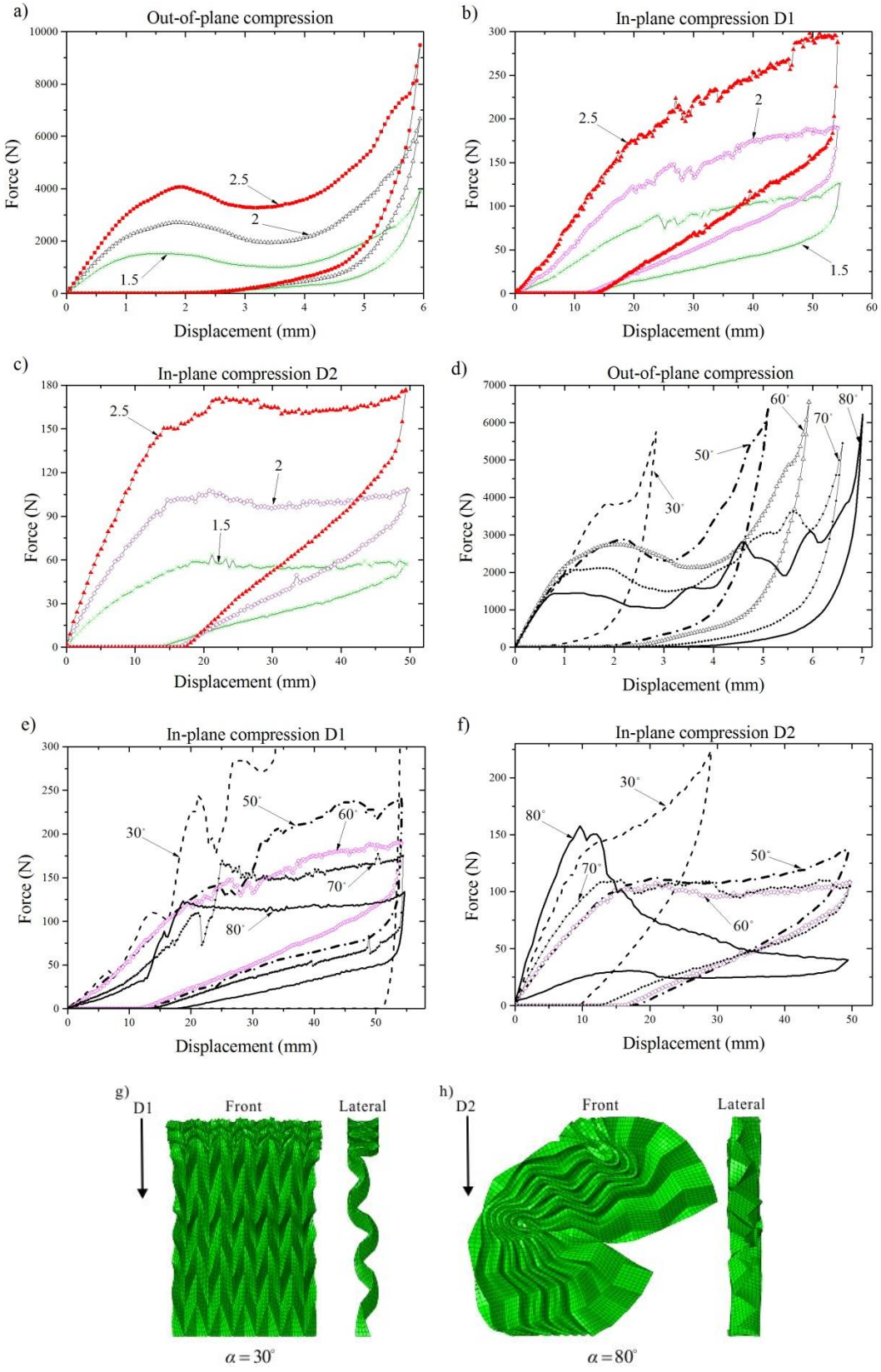

Figure 16 parallel parameter studies: thickness of facet *T*, a) out-of-plane compression, b) in-plane compression D1, c) in-plane compression D2; angle α, d) out-of-plane compression, e) in-plane compression D1, f) in-plane compression D2; the deformations of the sheet of g) $\alpha = 30^{\circ}$ in in-plane compression D1, h) $\alpha = 80^{\circ}$ in in-plane compression D2.